DUAL-POLARIMETRIC DECOMPOSITION OF SENTINEL-1 SAR IMAGE AND MACHINE LEARNING MODEL FOR OIL SPILL DETECTION: CASE OF MINDORO OIL SPILL

C. G. Candido[1,2*], J. A. Principe[1]

[1] Department of Geodetic Engineering, University of the Philippines – Diliman, Quezon City, Philippines– (cgcandido, japrincipe)@up.edu.ph

[2] Philippine Space Agency, 29th Floor, Cyber One Building, 11 Eastwood Ave., Bagumbayan, Quezon City, Philippines

KEY WORDS: Dual-polarimetric decomposition, Machine learning model, Mindoro, oil spill, Sentinel-1 SAR imagery

ABSTRACT:

Oil spills represent a significant environmental hazard necessitating timely detection to mitigate their detrimental effects. Synthetic Aperture Radar (SAR) technology serves as a remote sensing (RS)-based tool capable of detecting oil spills under varying weather conditions and at all times of day. SAR polarimetry, which assesses the polarization of the backscattered SAR signal, can effectively discriminate oil spills from other features that may manifest as dark regions in the SAR images. The integration of machine learning algorithms offers significant potential for enhancing the accuracy and efficiency of oil spill detection through SAR polarimetry. In recent years, several studies have introduced machine learning-based methodologies for this purpose, yet a comprehensive evaluation of their real-world performance remains essential. This study aimed to assess the efficacy of a machine learning (ML)-based approach for oil spill detection utilizing features derived from a dual-polarimetric decomposition method applied to Sentinel-1 SAR data. Results show that the machine learning-based approach achieved notable accuracy in oil spill detection reaching a score of 0.569 for intersection over union and 72.50 for f1-score of oil spill areas. Overall, this research underscores the potential of ML techniques as valuable tools for oil spill detection via SAR polarimetry.

1. INTRODUCTION

Oil spills are highly damaging to the environment and pose a serious threat to ecology and wildlife. Different sources of oil spill come from frequent illegal ship discharges or accidents involving tankers, barges, offshore platforms, and pipelines (Shirvany, Chabert, and Tourneret, 2012, Vijayakumar, 2022). The occurrence of oil spills in the ocean has emerged as a grave concern which has been particularly evident in the recent oil spill accident near the island of Mindoro, Philippines. The aftermath of the oil spill accident from the sunken tanker Princess Empress has inflicted enduring financial costs and burden and devastating marine life and creating serious ecological disaster in the area.

Accurate detection of oil spills is of great importance to protect marine life and environment, as well as to reduce economic losses caused by the oil spill. Synthetic Aperture RADAR (SAR) is a remote sensing technology that can be used to detect oil spills in all weather conditions and at any time of day. Electromagnetic waves are emitted and whose echoes are received by SAR sensors. Surface and capillary gravity waves are suppressed when oil slicks float on water's surface. This has an impact on the Bragg scattering of microwaves, which lowers the normalized radar backscatter cross-section (NRCS). This causes oil slicks to appear as dark areas on SAR images. However, other objects or phenomenon can also appear as dark spots on SAR images, such as low wind speed, natural surface films, cold upwelling water, divergent flow regimes, dry-fallen sand banks, discharge wastewater, or turbulent water. These oil spill look-alikes can lead to false detections, so it is important to distinguish these from actual oil spills (Alpers, Holt, & Zeng, 2017, Zhang, et. al., 2022).

Previous methods for oil spill detection used texture analysis of single-polarimetric SAR images. It can be broken down into a three-step process: (1) identification of dark areas, (2) extraction of features, and lastly (3) oil spill detection (Salberg & Larsen, 2018; Migliaccio, Gambardella, & Tranfaglia, 2007; Fingas & Brown, 2014). Due to the reliance on thresholding approaches and auxiliary external information, single-polarization methods are limited to their ability to detect oil spill (Migliaccio, Nunziata, and Buono, 2015).

The technological advancements of the space industry led to the launch of several high-performance SAR satellites that are equipped with polarimetric modes: X-band TerraSAR-X, L-band ALOS-2, the C-band Radarsat-2, and C-band Sentinel-1 satellite (Alpers, Holt, & Zeng, 2017). Significant contributions of SAR Polarimetry in oil spill detection were initially demonstrated by Migliaccio, Gambardella, and Tranfaglia (2007) and further supported by Migliaccio, Nunziata, and Gambardella (2009). Their research highlighted the crucial role of polarimetric information in detecting oil slicks and discriminating them from various oil spill look-alikes that characterized weak damping properties. Subsequently, several polarization decomposition methods have been employed in oil spill detection using quad- or dual-polarimetric SAR data, including methods like Cloude Decomposition, H/A/Alpha Decomposition, and Stokes parameters (Zhang, et. al., 2022). Another study by Salberg et. al., assessed various polarized parameters and classifiers for the purpose of oil spill detection, utilizing hybrid polarimetric SAR. Skrunes et. al. demonstrated that by analysing the geometric intensity and real component of the co-polarization cross-product of C-band SAR data, it was possible to effectively distinguish between biogenic oil slicks and mineral oil types.

In recent years, the emergence of machine learning and deep learning algorithms has led to the adoption in the field of polarimetric SAR oil spill detection. The gradual advancements of machine learning have resulted to the development of powerful and efficient algorithms that leverage the predictive potential of complicated datasets. A wide range of machine learning algorithms have been used for classification problem such as artificial neural network (ANN), support vector machine (SVM), decision tree (DT), and deep learning algorithms (Pujari, 2022).

* Corresponding author

Given the potential benefits that a machine learning algorithm and polarimetric decomposition might have to oil spill detection, the objective of this study was to assess the performance of a machine-learning based approach for oil spill detection with features derived from dual-polarimetric decomposition method of Sentinel-1 SAR data. Experiments were carried out on Sentinel-1 dual pol data. H/A/α dual decomposition method was used to generate the features that served as an input for the machine learning model, specifically the Extreme Gradient Boosting Machine. (Potin et. al., 2014).

2. STUDY AREA

2.1 Study Area

On the morning of February 28, 2023, the MT Princess Empress carrying 900,000 liters of industrial fuel oil sank off the coast of Naujan, Oriental Mindoro, Philippines. The spill affected the waters of the provinces of Antique, Batangas, Oriental Mindoro, and Palawan. The oil tanker was enroute from Limay, Bataan to Iloilo City when it experienced rough sea conditions and sank. The spill released 900,000 liters of industrial fuel oil into the sea, which is a highly toxic substance and spread quickly due to strong currents and winds and reached the shores of several coastal communities within days. The spill has had significant impact on marine life and coastal communities. It is the second largest oil spill in the Philippine history, after the 1996 Sea Empress Oil Spill (DENR, 2023). Fig. 1 shows the extent of the oil spill near Oriental Mindoro mapped by the Philippine Space Agency as of March 2023.

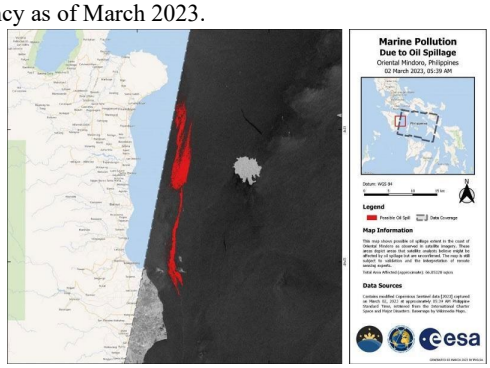

Figure 1. Oil Spill Map near Oriental Mindoro created by the Philippine Space Agency.

3. MATERIALS AND METHOD

The methodology is grouped into two major procedures: (1) Sentinel-1 image processing (Fig. 2), and (2) Model training and validation using Extreme Gradient Boosting Machine (XGBoost), Light Gradient Boosting Machine (LightGBM), and CatBoost (Fig. 3).

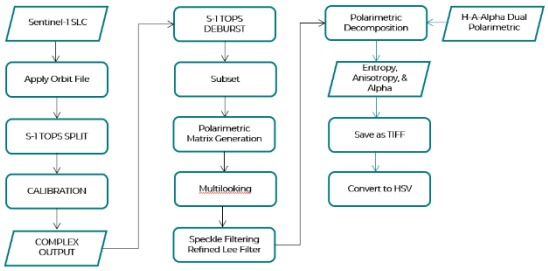

Figure 2. Schematic illustration showing the workflow for Sentinel-1 image pre-processing using SNAP.

3.1 Sentinel-1 Image Processing

3.1.1 Image Pre-processing

This study used the Copernicus Sentinel-1 Level 1 Single Look Complex (SLC) downloaded in the Copernicus Hub. Sentinel-1, equipped with a phase-preserving dual polarization SAR system, has the capability to capture multiple images within the same pulses using its antenna to receive specific polarization simultaneously. In this study, the Level-1 Single Look Complex (SLC) product which has a VH and VV polarization was acquired between the period of February to March 2023. SNAP was used to process the Sentinel-1 Level-1 SLC product. The SLC product contain complex values, enabling enhanced analysis of backscattering properties in addition to the measurement of backscatter intensity from each individual polarization. A radiometric calibration was first applied to the Sentinel-1 Level 1 SLC in which pixel values can be directly related to the scene backscattering. The image then undergoes De-bursting process, in which, individual scans are merged, and swath lines are removed. The resultant image was then further subdivided into a smaller area. After subdividing the image, a frequency domain multilook was applied to the image. This divides the bandwidth of the image into several parts called looks, each of which is used to form its own image. The images are then combined resulting to representation with a much greater Signal-to-noise (SNR) ratio at the given range solution. At this point all the image preprocessing which is needed for the decomposition process was completed.

3.1.2 Polarimetric Decomposition

The actual process of decomposition is started by creating a Polarimetric Matrix using SNAP's built-in Polarimetric Matrix Generation tool. This tool creates a matrix wherein each element of the matrix represents the backscatter response of the target in a particular polarization channel. Despite the significant decrease in signal-to-noise ratio caused by Polarimetric Matrix Generation, an additional speckle filtering was done and implemented using the Lee Refined Speckle Filtering. Geometric Terrain Correction was then applied to the image to reduce the level of distortion. A Polarimetric Decomposition process was then applied to the correctly oriented image which breaks down the image into Entropic, Anisotropic, and Alpha Decompositions. The image was then saved as GeoTIFF file and was converted into HSV color space to further enhance the contrast of oil spill from other resolvable features in the image (Figure 3).

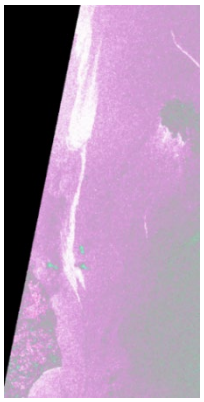

Figure 3. Geotiff file of the decomposed SAR image of Mindoro Oil Spill in HSV format

3.1.3 Dataset Tiling

The SAR dataset consisted of decomposed Sentinel-1 dual-pol SAR data from the Mindoro coast. The image was divided into small patches of 256 x 256 x 3 pixels for training, testing, and validation. A total of 242 images were generated from one single image.

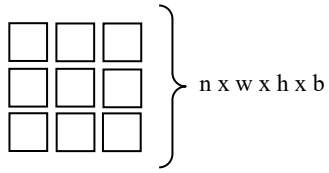

Figure 4. Structure of the dataset for model training and validation where n = tile number, w = number of rows, h = number of columns, and b = number of bands

The dataset was structured as such since one scene of the oil spill covers a very large area, classification of this image cannot be done without experiencing memory limitations. Thus, the image was tiled into 256 x 256 x 3 pixels.

3.2 Model Training and Validation

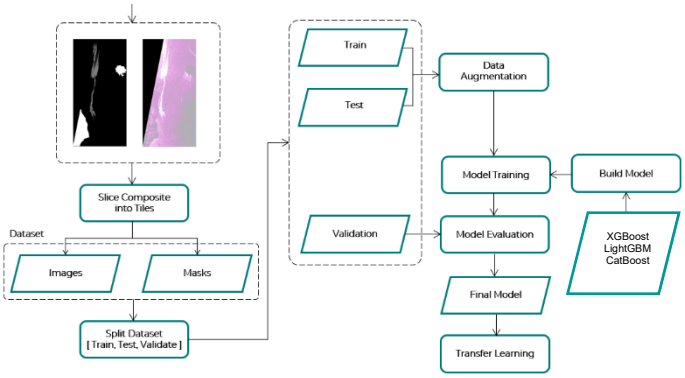

Figure 5. Schematic illustration showing the workflow for model training and validation.

3.2.1 Classification using Machine Learning Algorithm

Extreme Gradient Boosting Machine (XGBoost), Light Gradient Boosting Machine (LightGBM), and Categorical and Boosting (CatBoost) were used for the model training and validation of oil spill. The dataset used for model training were further split into training dataset and test dataset. The training dataset was used to train the machine learning algorithms and tune its hyperparameters and the test dataset was used to evaluate the models. The hyperparameters of the XGBoost, LightGBM, and CatBoost were determined from the training and test data using the randomized search approach based on 5-fold cross validation method. The RandomizedSearchCV method of the Sklearn Library implements a "fit" and "score", in which the model with a set of hyperparameters is fitted with the training dataset and the score of the model is evaluated using the test dataset. The process of fitting and evaluating is repeated until the optimal hyperparameters of XGBoost, LightGBM, and CatBoost were identified (Pedregosa, Varoquaux, Gramfort, and Thirion, 2011). Table 1 shows the hyperparameters of the XGBoost, LightGBM, and CatBoost that were tuned using the randomized search approach.

Model	Hyperparameters
XGBoost	max_depth
	learning_rate
	subsample
	colsample_bytree
	colsample_bylevel
	reg_alpha
	reg_lambda
	min_child_weight
	n_estimators
LightGBM	num_leaves
	min_child_samples
	min_child_weight
	subsample
	colsample_bytree
	reg_alpha
	reg_lambda
	n_estimators
CatBoost	depth
	iterations
	learning_rate
	l2_leaf_reg

Table 1. Hyperparameters of the XGBoost, LightGBM, and CatBoost tuned using the RandomizedSearchCV method.

Image patches were first converted to array and were stacked accordingly. The training dataset was then split into five folds; four folds were used to train model and the remaining fold was used to evaluate the model. The process of training and evaluation was repeated until all the folds were used as a test. The process was again repeated but with different set of hyper parameters. To prevent the model from over fitting, the best set of hyper parameters were selected based on cross-validation score. The hyperparameters of each machine learning algorithm that were tuned using the RandomizedSearchCV method are shown in Table 1.

3.3 Accuracy Assessment

The classification performances were estimated from the validation images that includes oil spill at different proportion. This accuracy metric was measured using Intersection over Union (IoU), F1-score, Precision, and Recall. Intersection over Union (IoU) is an evaluation metric used to measure the similarity between two sets of data. It quantifies the accuracy of the overlap between the predicted and the ground truth. The IoU is calculated as follows (Eq. 1):

$$\text{IoU} = (\text{Area of Intersection}) / (\text{Area of Union}) \quad (1)$$

The IoU can take on a value between 0 to 1. A value of 0 indicates that there is no overlap between the predicted and ground truth, while a value of 1 indicates that the predicted matches perfectly with the ground truth. The study also measured the pixel-wise precision, recall, and f1-score (Dice coefficient). The precision can be defined as follows:

$$Precision = \frac{True\ Positive}{True\ Positive + False\ Positive} \quad (2)$$

And the recall can define as given by:

$$Recall = \frac{True\ Positive}{True\ Positive + False\ Negative} \quad (3)$$

Lastly, the f1-score is defined as:

$$f1 - score = 2 * \frac{Precision * Recall}{Precision + Recall} \quad (4)$$

4. RESULTS AND DISCUSSION

A total of 227 image patches with a resolution of 256 x 256 x 3 were generated from one single image. The three-machine learning algorithm (XGBoost, LightGBM, and CatBoost) was trained and validated on the patched dataset via five-fold cross-validation. Model hyperparameters were selected based on the five-fold cross-validation of the training and test dataset. Table 2 shows the value of optimal hyperparameters for each machine learning algorithm.

Model	Hyperparameters	Optimal Values
XGBoost	max_depth	3
	learning_rate	0.5
	subsample	0.70
	colsample_bytree	0.70
	colsample_bylevel	0.60
	reg_alpha	0.5
	reg_lambda	5
	min_child_weight	5
	n_estimators	100
LightGBM	num_leaves	28
	min_child_samples	398
	min_child_weight	10.0
	subsample	0.75
	colsample_bytree	0.8814
	reg_alpha	0.1
	reg_lambda	1
	n_estimators	500
CatBoost	depth	10
	iterations	100
	learning_rate	0.01
	l2_leaf_reg	1

Table 2. Optimal values of hyperparameters for XGBoost, LightGBM, and CatBoost trained using 227 image patches and five-fold cross-validation.

Hyperparameter tuning is an essential component within the domain of machine learning. The choice of hyperparameters wield a significant impact on the performance of machine learning models. Several studies in the field (Bergstra and Bengio, 2012; Bergstra, et. al., 2011) have established that tuning of hyperparameters plays a vital role in improving model's accuracy, precision, and the capacity to generalize unseen data. Furthermore, hyperparameter tuning serves as a robust strategy for mitigating the issue of overfitting. Hyperparameter tuning operates as mechanism to find the trade-off between model complexity and simplicity, thereby reducing the susceptibility of machine learning models to overfitting (Chen, et. al., 2012).

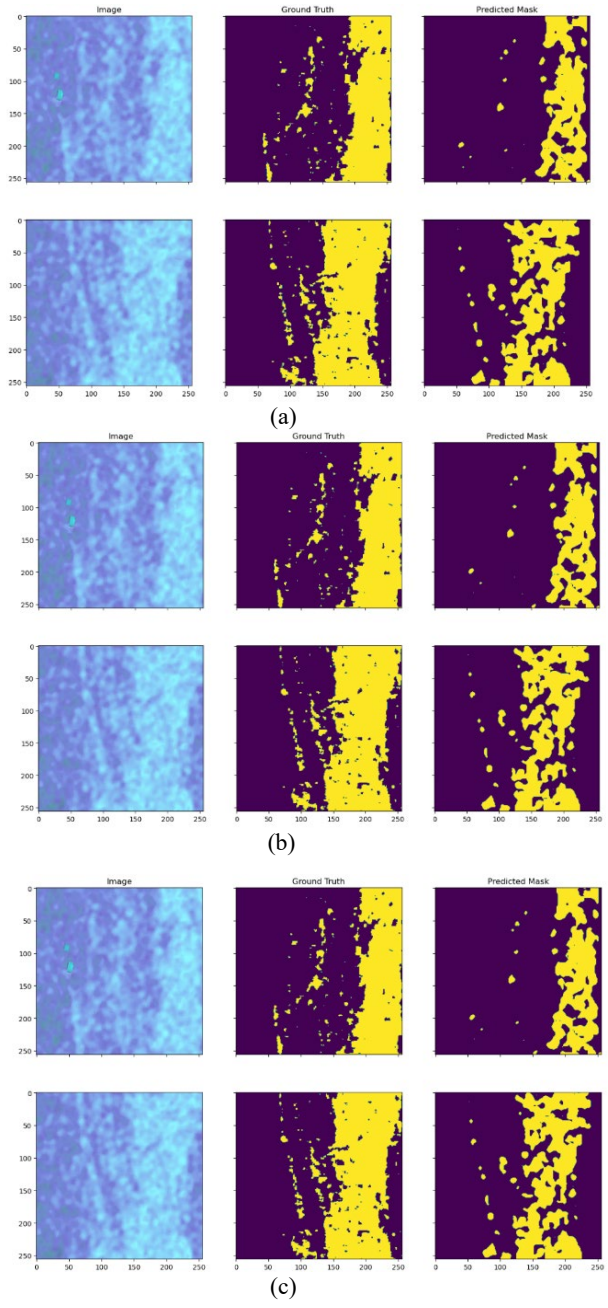

Figure 6. Binary-labelled classification maps from the decomposition of dual-pol S1 SAR images using (a) XGBoost, (b) LightGBM, and (c) CatBoost models. Yellow pixels are areas affected by oil spill.

Model	Image	Metric	Oil Spill	Non-Oil Spill
XGBoost	Image 1	Precision	90.390	87.000
		Recall	60.040	97.670
		f1-score	72.200	92.000
		IoU	0.565	
	Image 2	Precision	77.580	77.380
		Recall	54.550	90.790
		f1-score	64.100	83.500
		IoU	0.471	
LightGBM	Image 1	Precision	90.340	87.140
		Recall	60.550	97.640
		f1-score	72.500	92.100
		IoU	0.569	
	Image 2	Precision	77.540	77.500
		Recall	54.920	90.710
		f1-score	64.300	83.600
		IoU	0.474	
CatBoost	Image 1	Precision	90.730	86.860
		Recall	59.510	97.780
		f1-score	71.900	92.000
		IoU	0.561	
	Image 2	Precision	77.560	77.180
		Recall	53.990	90.880
		f1-score	63.700	83.500
		IoU	0.467	

Table 3. Evaluation metrics of dual-polarimetric decomposition and three machine learning models (XGBoost, LightGBM, and CatBoost) using precision, recall, f1-score (dice coefficient), and intersection over union

The binary-labelled maps, which were classified from the decomposition of dual-polarimetric Sentinel-1 SAR images by XGBoost, LightGBM, and CatBoost models, was seen in Fig. 6. Significant difference could not be found in the three classification maps. Several oil spill areas were classified as non-oil spill by the three machine learning models. The general shape of the oil spill was properly delineated for the three machine learning models. Table 3 shows the evaluation metrics intersection over union, precision, recall, and f1-score (dice coefficient) for each machine learning models.

Based on Table 3, the IoU score ranges between the values of 0.467 to 0.569. The LightGBM model produced the highest IoU among the machine learning models for both the two validation images with a score of 0.569 and 0.474. Although, LightGBM achieved the highest IoU score, there is no significant difference among the other two machine learning models. Furthermore, it is evident among the machine learning models that the recall of oil spill areas achieved low scores. Low recall in classification accuracy means that the model is not effectively identifying a substantial portion of the actual positive instances which means that there is a high rate of false negatives. Recall, also known as sensitivity, measures the model's ability to correctly identify all positive instances. When recall is low, the model is missing significant positive instances which could be problematic. This is accurately portrayed on the labelled image of each model, wherein, the area of oil spill for the predicted mask is significantly lower compared to the actual or ground truth.

In this study, the challenge of detecting oil spills from the decomposition of dual-polarimetric Sentinel-1 SAR images was addressed using three different machine learning models. Our approach relies on the utilization of features generated by the H/A/α dual polarimetric decomposition (Entropic, Anisotropic, and Alpha) as opposed to the traditional approach which employs textural features and other features as input data for the classification.

Polarimetric features derived from the decomposition were used as input for the oil spill classification since they are directly related to the physical properties of the scattering of the surface. The polarimetric scattering characteristics of the oil-covered sea surface depends on several contributing factors such as substance type, SAR instrument specific parameters (polarization, incidence angle, noise floor), and geophysical parameters (wind, presence of capillary waves, surface currents). The notion of using polarimetric SAR data for oil spill detection was initially examined by Gade et. al., and was subsequently demonstrated on fully polarimetric ALOS PALSAR data by Migliaccio, et. al.

The study of Migliaccio, et. al. proposed Eigenvalue decomposition as a method for oil spill detection. Eigenvalue - based polarimetric features (Entropy, Anisotropy, and Mean Scattering Angle) are used to classify oil spills using a single SIR-C/X-SAR L-band dataset. While the classical H/A/α parameters in the fully polarimetric case also offers physical insights (predominant scattering), it is essential to acknowledge that they only capture a portion of the complete physical phenomena of the scatterer. In the case of oil-covered sea surface, Entropy tends to zero, therefore it is a dominant scattering mechanism scenario. On the other hand, pollution-free sea surface is dominated by relative high Entropy, representing random scattering mechanisms (Singha, et. al., 2016).

Based on the results, the following can be concluded: (i) polarimetric features (entropy, anisotropy, and mean scattering angle) derived from the decomposition of dual-polarimetric Sentinel-1 SAR image could be used to classify oil spill; (ii) combining polarimetric features with machine learning models could be an alternative approach in detecting oil spill as opposed to using textural features or intensity; and (iii) The machine learning models produced an IoU score ranging from 0.467 to 0.569, and an f1-score for oil spill areas ranging from 63.70 to 72.50, with LightGBM model producing the highest IoU and f1-scores.

5. CONCLUSION

In this study, polarimetric features derived from the decomposition of dual-polarimetric Sentinel-1 SAR image was used in combination with machine learning model to identify oil spill. The methodology starts with the decomposition of Sentinel-1 SAR images using the H/A/α decomposition method. The resulting image was split into patches of 256 x 256 x 3. Image patches are then provided to the three machine learning models (XGBoost, LightGBM, and CatBoost) that was trained on 80.0% of the patches and was validated via five-fold cross-validation. LightGBM achieved the highest accuracy among the three machine learning models with a value of 0.569 for IoU and 72.50 for f1-score in oil spill labels.

AKNOWLEDGEMENT

The author would like to thank Philippine Space Agency – Space Data Mobilizations and Applications Division for their invaluable assistance in this research endeavour. The provision of ground truth data for the Mindoro oil spill was instrumental in ensuring the accuracy and reliability of the findings of the study.

REFERENCES

Alpers, W., Holt, B., and Zeng, K., 2017. Oil spill detection by imaging radars: challenges and pitfalls. *Remote Sensing of Environment*, 201, 133-147

Baek, W.K., Jung, H.S., 2021. Performance comparison of oil spill and ship classification from x-band dual- and single-polarized SAR Image using support vector machine, random forest, and deep neural network. *Remote Sensing*, 13(16), 3203

DENR., 2023. MT Princess Empress oil spill updates. URL https://www.denr.gov.ph/index.php/news-events/mt-princess-empress-oil-spill-updates (Accessed 06.29.2023)

Fingas, M.F., and Brown, C.E., 2014. Chapter 12 - oil spill remote sensing. *Handbook of Oil Spill Science and Technology*, 311-356, https://doi.org/10.1002/9781118989982.ch12

Migliaccio, M., Nunziata, F., and Buono, F., 2015. SAR polarimetry for sea oil slick observation. *International Journal of Remote Sensing*, 36(12), 3243-3273

Migliaccio, M., Gambardella, A., and Tranfaglia, M., 2007. The PALSAR polarimetric mode for sea oil slick observation. *IEEE Transactions on Geoscience Remote Sensing*, 45, 506-511

Pedregosa, F., Varoquaux, G., Gramfort, A., Michel, V., Thirion, B., Grisel, O., Blondel, M., Prettenhoffer, P., Weiss, R., Dubourg, V., Vanderplas, J.; Passos, A.; Cournapeau, D., Brucher, M., Perrot, M., and Duchesnay, E., 2011. Scikit learn: Machine Learning in Python. *Journal of Machine Learning Research*, 12, 2825-2830

Potin, P., Rosich, B., Roeder, J., and Bargellini, P., 2014. Sentinel-1 mission operations concept. *IEEE Geoscience and Remote Sensing Symposium*, 1465-1468

Pujari, P., 2023. Comparative study of machine learning classifiers for oil spill classification: assessing the effectiveness of Random Forest and XGBoost. *Journal of Emerging Technologies and Innovative Research*, 10(6), 508-515

Ronneberger, O., Fischer, P., & Brox, T., 2015. U-Net: convolutional networks for biomedical image segmentation. 18th *International Conference on Medical image Computing and Computer-assisted Intervention*, III (18), 234-241

Salberg, A.B., Larsen, S.O., 2018. Classification of ocean sea surface slicks in simulated hybrid-polarimetric SAR images. *IEEE Trans. Geosci. Remote Sensing*, 52, 6521-6533

Singha, S., Ressel, R., Velotto, D., and Lehner, S., 2016. A Combination of traditional and polarimetric features for oil spill detection using TerraSAR-X. *IEEE Journal of Selected Topics in Applied Earth Observations and Remote Sensing,* 1-12

Shirvany, R., Chabert, M., and Tourneret, J.Y., 2012. Oil spill detection using degree of polarization in linear and hybrid/compact dual-pol SAR. *IEEE Journal of Selected Topics in Applied Earth Observations and Remote Sensing*, 5(3), 885-892

Skrunes, S., Brekke., C., Eltoft, T., 2014. Characterization of marine surface slicks by RADARSAT-2 multipolarization features. *IEEE Trans. Geosci. Remote Sens.*, 52, 5302-5319

Vijayakumar, S., 2023. Computational techniques of oil spill detection in synthetic aperture radar data: review cases. IntechOpen. doi: 10.5772/intechopen.108115

Zhang, J.Z., Feng, H., Luo, Q., Li, Y., Zhang, Y., Li, J., and Zeng, Z., 2022. Oil spill detection with dual-polarimetric Sentinel-1 SAR using superpixel-level image stretching and deep-convolutional neural network. *Remote Sensing*, 14(6), 3900